*Antarctic Science 12 (4): 429–442 (2000)* © British Antarctic Survey Printed in the United Kingdom

# SHRIMP U–Pb geochronology from Mount Kirkby, northern Prince Charles Mountains, East Antarctica

**C.J. CARSON[1]*, S.D. BOGER[2], C.M. FANNING[3], C.J.L. WILSON[2] and D.E. THOST[4]**

[1]*Department of Geology and Geophysics, Yale University, New Haven, CT 06511, USA*
[2]*School of Earth Sciences, University of Melbourne, Parkville, VIC 3052, Australia*
[3]*Research School of Earth Sciences, Australian National University, Canberra, ACT 0200, Australia*
[4]*Australian Antarctic Division, Kingston, TAS, 7050, Australia*
**carson@hess.geology.yale.edu*

**Abstract:** Sensitive High Resolution Ion MicroProbe (SHRIMP) U–Pb zircon dating of pegmatites from Mount Kirkby, northern Prince Charles Mountains, east Antarctica indicates felsic intrusive activity at 991 ± 22 Ma and 910 ± 18 Ma. Pegmatite emplacement occurred during prolonged high-grade early Neoproterozoic tectonism. These ages correlate well with previously published U–Pb zircon ages obtained from felsic intrusive bodies elsewhere within the northern Prince Charles Mountains. Early Palaeozoic activity at Mount Kirkby is restricted to the emplacement of minor planar pegmatites at 517 ± 12 Ma, which provide a maximum age for local development of discrete extensional mylonites. No conclusive evidence of tectonic or metamorphic events at *c.* 800 Ma and *c.* 500 Ma, which have been recently postulated for the region, can be identified from the presently available U–Pb zircon data.

Received 8 September 1999, accepted 15 May 2000

**Key words:** Early Palaeozoic, early Neoproterozoic, East Antarctica, northern Prince Charles Mountains, SHRIMP

## Introduction

The East Antarctic Shield (EAS) is a complex mosaic of metamorphic terranes ranging in age from Archaean to early Palaeozoic, and has received considerable geological attention during the past three decades (e.g. Tingey 1991). Modern geochronological investigations in the EAS have not only resulted in improved resolution of the gross distribution of metamorphic terranes but have refined the internal chronological evolution within individual terranes. In many regions of the EAS, however, the geochronological database remains relatively limited, restricting continued refinement of regional geological models.

The northern Prince Charles Mountains (nPCM), located in the EAS between latitudes 70–72°S and longitudes 60–70°E (Fig. 1), represent a large region of high-grade metamorphic rocks long recognized to be part of an extensive high-grade orogenic terrane that evolved at *c.* 1000 Ma (e.g. Arriens 1975, Tingey 1982, Manton *et al.* 1992, Kinny *et al.* 1997, Boger *et al.* in press). However, the recent identification of pervasive early Palaeozoic granulite–facies tectonism in nearby Prydz Bay (Zhao *et al.* 1992, Hensen & Zhou 1995, Carson *et al.* 1996, Fitzsimons *et al.* 1997) has led to conjecture addressing the possibility of an early Palaeozoic high-grade metamorphic overprint in the nPCM region (e.g. Hand *et al.* 1994a, Zhou & Hensen 1995, Carson *et al.* 1996, Hensen *et al.* 1997, Scrimgeour & Hand 1997). Hensen *et al.* (1997) also proposed that a high-grade metamorphic event affected the nPCM at *c.* 800 Ma. The possibility that several metamorphic episodes affected the nPCM from the earliest Neoproterozoic to the early Palaeozoic and a relatively limited structurally-constrained geochronological database, render it problematic to fully assess the absolute timing of various structures across the region. Resolving the chronology, nature and intensity of these metamorphic events is essential for development of regional tectonic models.

In this paper new SHRIMP U–Pb zircon geochronological data for four samples from Mount Kirkby (Fig. 1) are presented in the context of the local structural evolution. These data provide additional information on the nature and duration of the *c.* 1000 Ma event and provide context for further debate on the extent, intensity and structural manifestation of post-1000 Ma metamorphic events in the nPCM. This information also provides an important temporal framework for the correlation of high-grade structures across the nPCM and nearby regions.

## Geological setting

The nPCM represent one of the most extensive exposures of early Neoproterozoic (*c.* 1000 Ma) granulite–facies rocks in the EAS. The region is exposed to the west of the Lambert Glacier, (Fig. 1) and consists of three east–west trending ranges of flat-topped massifs and nunataks, (the Athos, Porthos and Aramis ranges), and the massifs of the Amery Oasis region adjacent to Beaver Lake (Fig. 2). During the early Neoproterozoic, the region experienced peak metamorphic conditions of *c.* 6–7 kbar at *c.* 700–800°C (e.g. Fitzsimons & Thost 1992, Fitzsimons & Harley 1994a, 1994b, Thost &

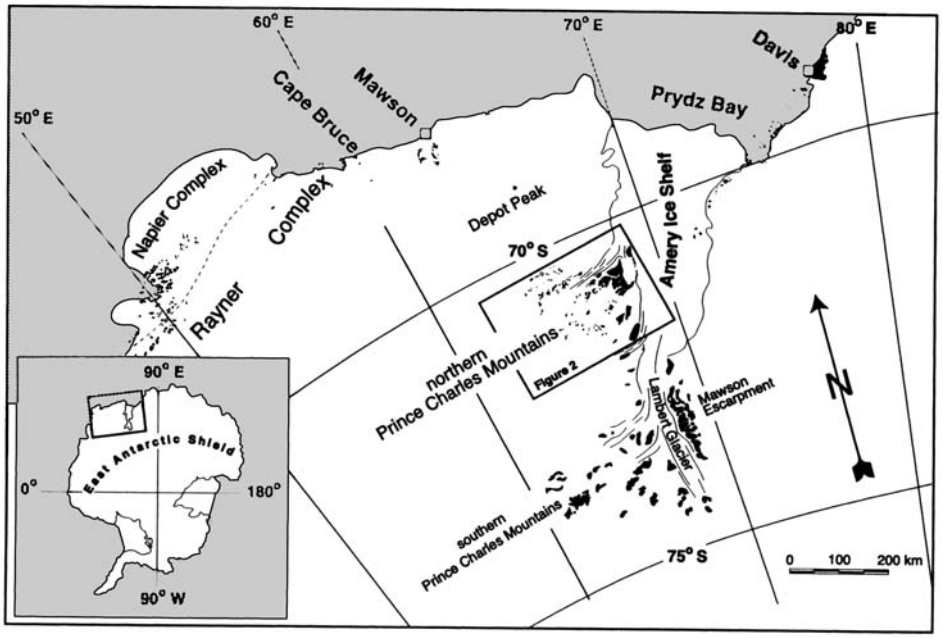


**Fig. 1**. Location map of the regions discussed in the text. The nPCM region is indicated and enlarged in Fig. 2.

Hensen 1992, Scrimgeour & Hand 1997), with most workers describing a cooling-dominated retrograde *P–T* history (e.g. Fitzsimons & Harley 1992, 1994a, 1994b, Nichols 1995, Stephensen & Cook 1997, cf. Hand *et al.* 1994a).

The nPCM have been correlated, by age and metamorphic grade, with the early Neoproterozoic (*c.* 1000 Ma) Rayner Complex of Kemp Land and Enderby Land (e.g. Black *et al.* 1987, Harley & Hensen 1990, Fitzsimons & Thost 1992,

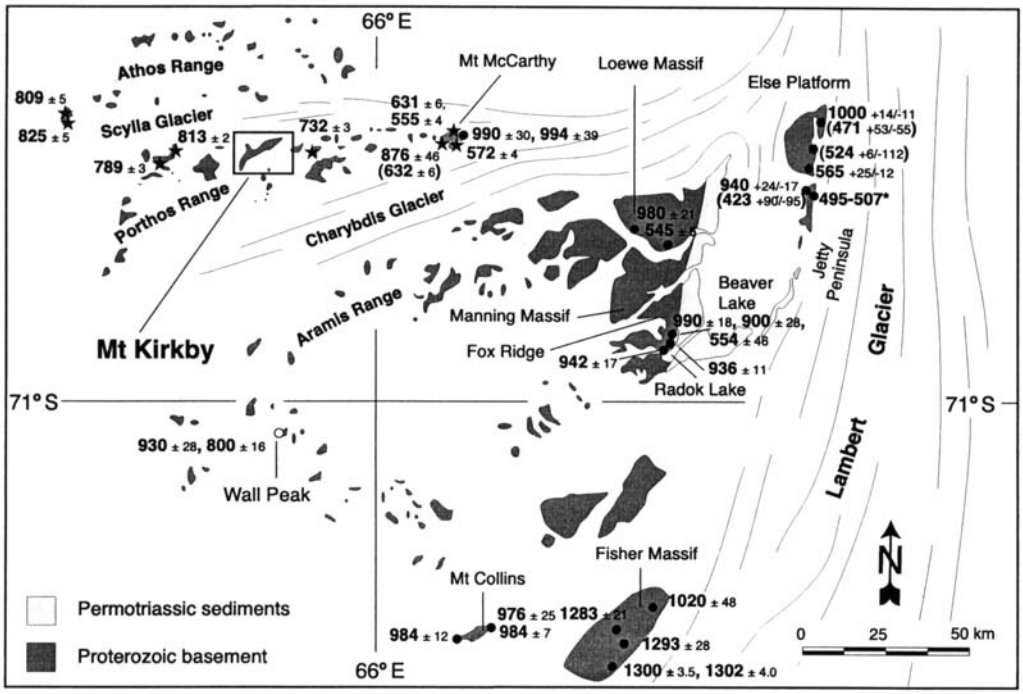


**Fig. 2.** Map of the northern Prince Charles Mountains region. The study area, Mount Kirkby, is shown. The solid circles indicate sites of samples dated by U–Pb zircon geochronology, with the ages shown next to each site (Manton *et al.* 1992, Beliatsky *et al.* 1994, Kinny *et al.* 1997, Boger *et al.* in press, Boger unpublished data). The bracketed ages on Jetty Peninsula represent U–Pb lower intercepts. *No errors given by Manton *et al.* (1992). Open circle at Wall Peak represents Th–Pb ages on monazite (Nichols & Fahey 1996). Solid stars indicate site of samples dated by Sm–Nd garnet–whole rock isochron analysis (Hensen *et al.* 1997). The results shown are for leached garnet fractions. The bracketed age at Mount McCarthy is a Sm–Nd garnet–whole rock isochron age for the growth of garnet coronas in a mafic unit.

https://doi.org/10.1017/S0954102000000523 Published online by Cambridge University Press

Fitzsimons 2000), where it is bounded to the north by the Archaean Napier Complex. The nPCM are bounded to the east by the Lambert Graben; north-east of this lies the early Palaeozoic high-grade terrane of south-western Prydz Bay. South of the nPCM at Fisher Massif, the metamorphic grade is lower-amphibolite facies (e.g. Kamenev *et al.* 1993, Crowe 1994, Beliatsky *et al.* 1994). Further south, the southern Prince Charles Mountains (sPCM) is exposed (e.g. Tingey 1982, 1991). This poorly understood polymetamorphic terrane is composed of Archaean orthogneiss basement overlain by Archaean and Proterozoic metasediments and intruded by Cambrian granite stocks and pegmatites. The geological relationships between the Fisher Massif metavolcanic sequences, the sPCM and the high-grade exposures in the nPCM (Fig. 1) are currently unclear. However, based on geochemical evidence at Jetty Peninsula and field and petrological observations at Radok Lake, Manton *et al.* (1992) and Boger *et al.* (in press) propose that the nPCM granulites are allochthonous, and are thrust over low-grade units that may be equivalent to the units exposed at Fisher Massif.

Mount Kirkby, the focus of this study, is located near the western end of the Porthos Range (Figs 2 & 3). Like much of the northern Prince Charles Mountains, Mount Kirkby is composed of orthopyroxene-bearing quartzo-feldspathic orthogneiss, with minor mafic gneiss and psammitic lenses. Mount Kirkby is intruded by minor pre-, syn- and post-tectonic felsic pegmatites, minor garnet-bearing leucogneiss (Fig. 3) and planar mafic dykes which also post-date high-grade activity (e.g. Fitzsimons & Thost 1992).

*Structure*

Several structural schemes have been proposed for the nPCM, resulting in minor differences in structural nomenclature across the region. However, high-grade structures in the nPCM are relatively straightforward and easily identifiable across the region, allowing reliable regional correlation. For the purposes of this paper a simplified nomenclature will suffice (after Boger *et al.* in press), describing the major structural features of the region (Table I). We present this structural framework in the context of the geochronological investigations presently available; the geochronological results of this study will be presented in a later section.

A regional gneissosity, here termed $S_1/S_0$, was produced during $D_1$. $S_1/S_0$ was originally flat-lying (e.g. Fitzsimons & Thost 1992, Boger *et al.* in press) and truncates folded fabrics in small mafic and ultramafic boudins (Fitzsimons & Thost 1992, Thost & Hensen 1992). $S_1/S_0$ contains a variably developed, shallowly east (or west) plunging stretching mineral lineation, $L_1$, defined by rodded quartz and feldspar, which is sub-parallel to rare rootless intrafolial isoclinal $F_1$ folds. $S_1/S_0$ is deformed to rare, originally recumbent, $F_2$ isoclinal folds, that are co-linear with $L_1$.

The major structural episode that controls the macroscopic geometry of the nPCM is characterized by open to tight folding ($F_3$) of the regional gneissosity forming large (kilometre-

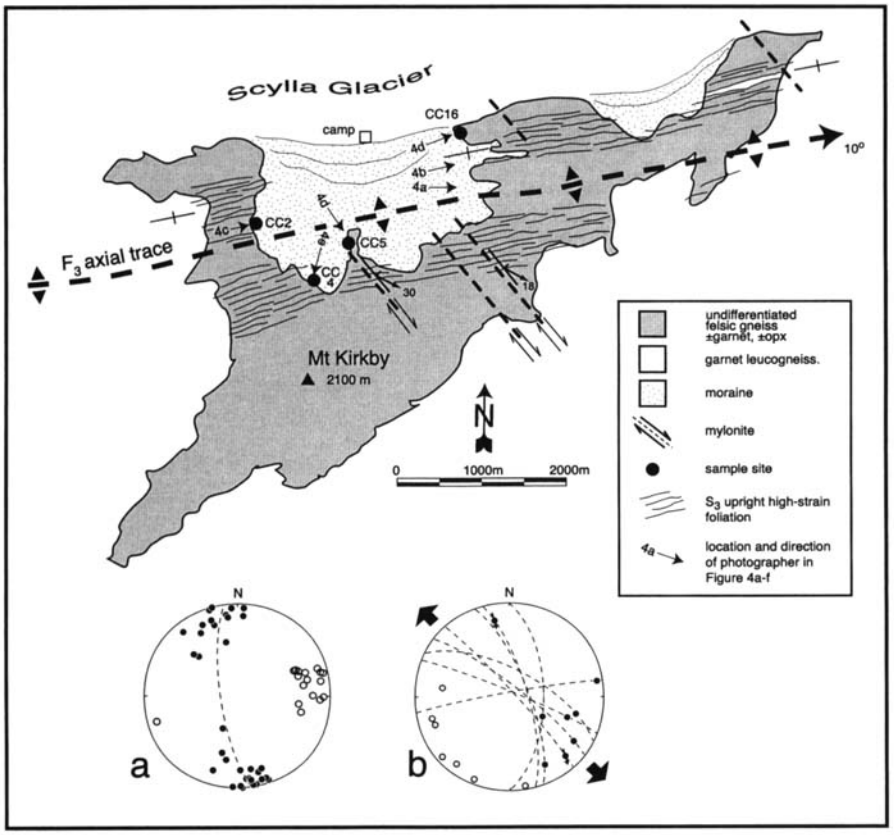


**Fig. 3.** Schematic map of Mount Kirkby, showing the general structural features and sample locations discussed in the text. The numbered arrows indicate the location, and viewing direction of the photographs displayed in Fig. 4a–f. The insets (equal area, lower hemisphere projections) show: **a.** the distribution of poles to $S_3$ (filled circles $n = 41$) and the $L_1$, $L_3$ mineral lineation (open circles, $n = 18$). **b.** Mylonite orientations are illustrated as great circles and as poles to mylonite surfaces (open circles, $n = 7$). Filled circles are lineations on mylonite planes. Small arrows indicate the movement direction of the hanging wall block. Large arrows indicate the extension direction (after Oncken 1988).

https://doi.org/10.1017/S0954102000000523 Published online by Cambridge University Press

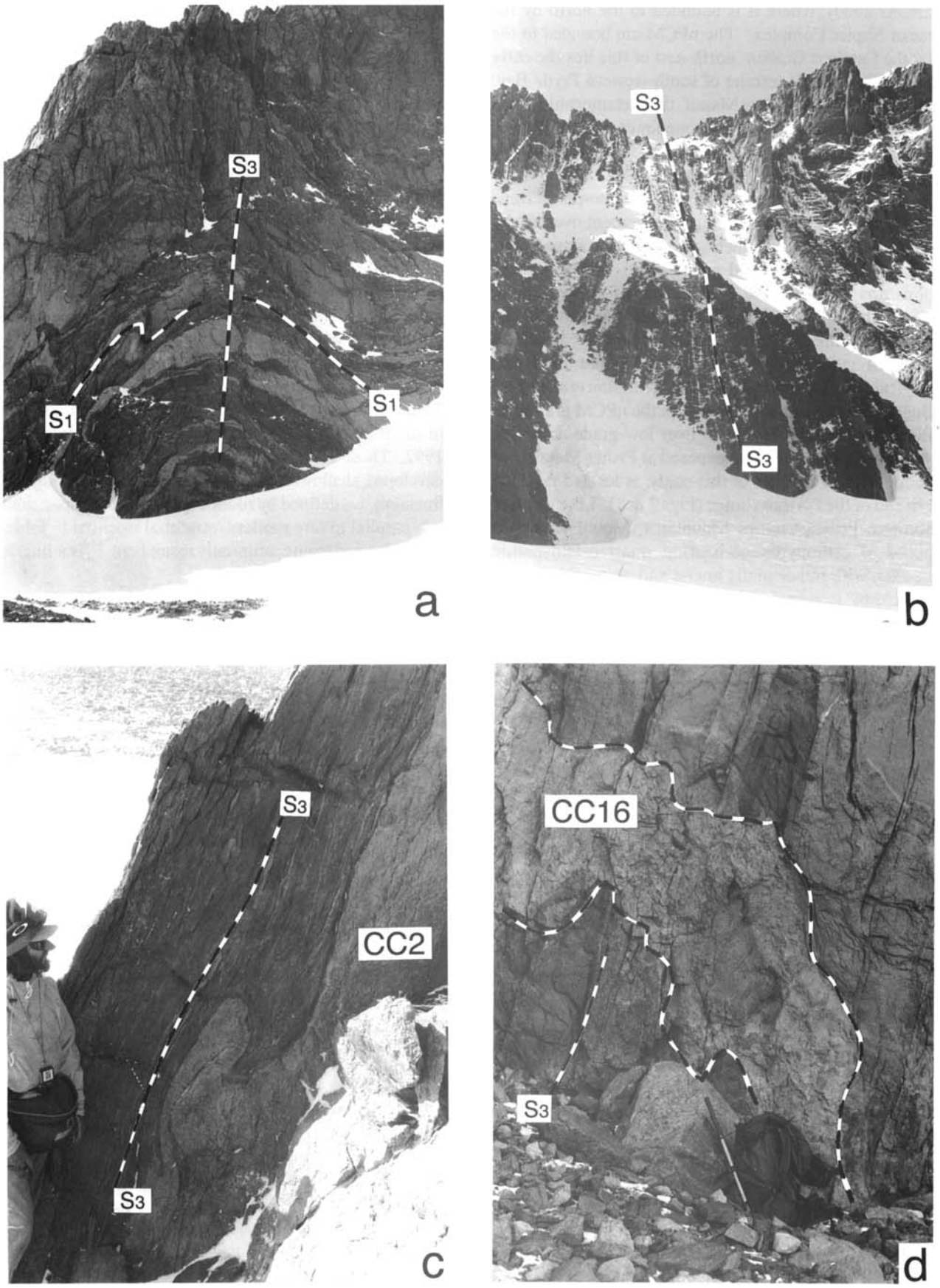


https://doi.org/10.1017/S0954102000000523 Published online by Cambridge University Press

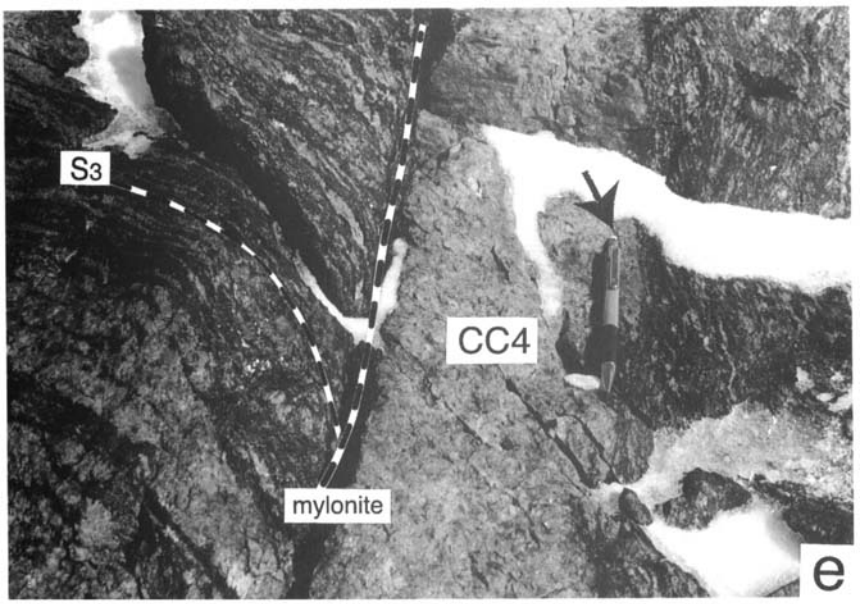


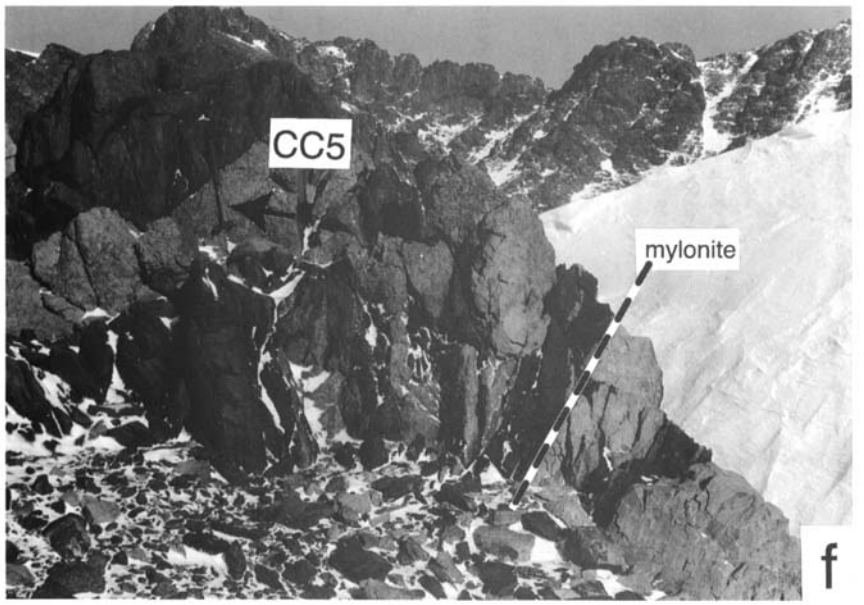


**Fig. 4.** (and opposite) Field photographs of structural features at Mount Kirkby. **a.** Fold hinge of a major $F_3$ fold, photographer facing east. Base of cliff *c.* 100 m. **b**. Upright high-strain $S_3$ foliation, *c.* 200 m north of previous photograph. Base of cliff *c.* 150 m. **c.** Transposed pegmatite (sample CC2) located within high-strain $S_3$ foliation. Base of photo *c.* 2.5 m. **d**. South-dipping pegmatites (sample CC16) crosscutting upright–steeply inclined $S_3$ foliation. Note that the pegmatite is weakly folded, with axial planes parallel to $S_3$ and crosscuts isoclinal $F_3$ folds in the high-strain foliation. Base of cliff *c.* 5 m. **e**. Planar pegmatite (sample CC4), with margins reworked by discrete mylonites. Pen (arrowed) for scale is *c.* 100 mm long. **f**. Planar pegmatite (sample CC5) deformed by mylonite (indicated). Sledgehammer for scale (arrowed), handle *c.* 1 m long.

scale) symmetrical, cylindrical upright antiforms (Fig. 4a). At Mount Kirkby, the trace of an $F_3$ antiform runs along the east–west axis of the massif (Fig. 3). No $S_3$ axial planar fabric is developed in $F_3$ fold hinges. However, the limbs of $F_3$ structures are commonly attenuated into steep to vertical, east–west trending, tabular zones of high-strain, up to hundreds of metres wide, where a new gneissosity ($S_3$) is developed (Fig. 4b & c), parallel to the axial plane of $F_3$ (e.g. Fitzsimons & Thost 1992). A generation of relatively undeformed south-dipping pegmatites was emplaced late syn-$D_3$ (Fig. 4d; described below). A mineral elongation lineation, $L_3$, is variably developed on $S_3$, and is indistinguishable in orientation and appearance from $L_1$ preserved on $S_1/S_0$ surfaces within zones of $D_3$ low-strain. At Mount Kirkby, $L_3$ plunges shallowly to the east (Fitzsimons & Thost 1992, this study) and is co-linear with $F_1$, $F_2$ and large-scale $F_3$ fold hinges. Wide mylonitic zones, that sub-parallel $S_3$ high-strain zones and show reverse sense of movement, are located on Fox Ridge and Mount Kirkby (south over north, unpublished field data), Else Platform (Hand *et al.* 1994b) and Manning Massif, and appear to result from increased partitioning of strain at lower conditions during waning $D_3$. The reader is referred to the illustrative block diagrams presented in fig. 2 of Thost & Hensen (1992), fig. 6 of Fitzsimons & Harley (1992) and fig. 12 of Boger *et al.* (in press) for a visual summary of the high-grade structural relationships.

Discrete mylonites, ultramylonites and pseudotachylyte generations (e.g. Thost & Hensen 1992, Fitzsimons & Thost 1992, Hand *et al.* 1994b, Nichols 1995) (Fig. 4e & f) are widespread in the nPCM region and have been assumed by most workers to represent structural development during the early Palaeozoic (cf. Nichols & Fahey 1996). At Mount

https://doi.org/10.1017/S0954102000000523 Published online by Cambridge University Press

**Table I.** Preferred correlation of structural schemes and U–Pb age determinations for the northern Prince Charles Mountains region.

| U–Pb zircon age determinations | Fitzsimons & Thost (1992) (western nPCM) | Thost & Hensen (1992) (western nPCM) | Hand *et al.* (1994b) (Else Platform) | Nichols (1995) (south-western nPCM) | Boger *et al.* (in press) (Radok Lake) | This study (Mount Kirkby; Porthos Range) |
|---|---|---|---|---|---|---|
| ?unknown > 1000Ma? | $D_1$–$D_2$; development of $S_1$& S2 as folded fabric within mafic and ultramafic pods | $D_1$–$D_2$, development of $S_1$& $S_2$ as folded fabric within mafic and ultramafic pods | not described | not described | not described | not described |
| *c.* 1000 Ma §†¥ | $D_3$; formation of regional flat-lying $S_3$ gneissosity | $D_3$; formation of regional $S_3$ flat-lying gneissosity | $D_1$; development of regional $S_1$ gneissosity; formation of isoclinal F1 folds | $D_1$; development of regional $S_1$ gneissosity; **MY1** development; $D_2$; $F_2$ isoclinal folds | $D_1$; development of regional $S_1$ gneissosity; formation of intrafolial isoclinal F1 folds | $D_1$; development of regional $S_1$ gneissosity; formation of intrafolial isoclinal $F_1$ folds |
| 990 ± 18 Ma ¥ | $D_4$; folding of $S_3$ into $F_4$ isoclines | $D_4$; folding of $S_3$ into $F_4$ isoclines | not described | See footnote[1] | $D_2$; folding of $S_1$ into recumbent isoclines | $D_2$; folding of $S_1$ into rare recumbent to inclined isoclines |
| 980 ± 21 Ma ¶<br>990 ± 30 Ma ¶ | EMPLACEMENT OF CHARNOCKITE (LOEWE MASSIF) AND GARNET-BEARING LEUCOGNEISS (MT McCARTHY) | | | | | |
| | $D_5$; small-scale (< 150 mm) open to tight folding | not described | not described | not described | not described | not described |
| 991 ± 22 Ma° ↓ *c.* 940 Ma ¥† 910 ± 18 Ma° | $D_6$; Regional east–west upright folding; development of upright high-strain zones | $D_5$; Regional east-west upright folding; developmentof upright high-strain zones | $D_2$; Upright to steep east–west trending folding; development of steep south-dipping east–west trending high-strain zones | $D_3$; Upright east–west trendingfolding; development of upright high-strain zones[1] **MY2** development, e.g. Fox Ridge shear zone. | $D_3$; Upright to steep, east–west trending folding; development of steep south-dipping high-strain zones | $D_3$; Upright east–west trending folding; development of upright high-strain zones development of north-dipping high-strain zones. |
| 900 ± 28 Ma ¥ | $D_7$; shear zones and minor flexures (assumed >750 Ma) | $D_6$; shear zones and minor flexures (intruded by planar pegmatite dykes) | $D_3$; NNE trending mylonites, steep east-dipping, reverse movement. (assumed *c.* 500 Ma) | **MY3**; low angle normal faults with easterly transport direction | $D_4$; NE–SW trending mylonites /pseudotachylytes, low angle thrusts at Radok Lake *(predating* planar pegmatites and associated mylonite development). | not described |
| <517 ± 12 Ma°<br><545 ± 4 Ma ‡ | $D_8$; mylonites and pseudotachylytes postdating planar pegmatites (assumed ~500 Ma) | $D_7$; mylonites and pseudotachylytes postdating planar pegmatites. | $D_4$; discrete mylonite and ultramylonite generations (assumed *c.*500–485 Ma in age) | Greenschist-facies retrograde shear zones (RSZ; assumed *c.* 500 Ma) | Post-900 Ma mylonites which postdate *c.* 550 Ma planar pegmatites‡, predate *c.* 475 Ma Rb-Sr biotite ages‡. | Discrete mylonite and ultramylonite generations postdating planar pegmatites. |
| 308–119 Ma[2] ∞ | Quartz and epidote veins | Quartz and epidote veins | Late north–south brittle features | Brecciated calcite and quartz veins | not described | Quartz and calcite veins |

Geochronological references: § Tingey (1982), ∞ Hoffman (1991), † Manton *et al.* (1992), ¶ Kinny *et al.* (1997); ¥ Boger *et al.* (in press), ‡ Boger unpublished data, °This study. 1. Nichols (1995) places his $D_3$ (upright macroscopic folds) *prior* to the emplacement of the Loewe Massif Charnockite; most workers conclude that the upright folding event and synchronous development of steeply dipping high-strain zones occurred *after* or *late-syn* charnockite emplacement. 2. Age constraints on the brittle quartz-epidote-calcite veins based on Hoffman (1991). Hoffman (1991) describes mafic dykes in the Else Platform region (K–Ar whole-rock age = 308 ± 10 Ma) which are brecciated and crosscut by quartz veins, which are in turn crosscut by Early Cretaceous monchiquites (K–Ar whole rock age = 119 ± 6 Ma).





https://doi.org/10.1017/S0954102000000523 Published online by Cambridge University Press

Kirkby, discrete mylonite sets typically trend north-west, dip moderately north-east and display dextral strike-slip motion with a minor extensional component along a shallowly south-east-pitching mineral lineation (Fig. 3). These features deformed the margins of planar pegmatites (Fig. 4e) in some cases.

*Previous geochronology*

The first geochronological investigation conducted in the nPCM was the Rb–Sr whole rock and mineral isochron study of Arriens (1975, recalculated by Tingey 1982) which yielded ages that clustered around 900–1000 Ma. Manton *et al.* (1992) obtained a U–Pb concordia upper-intercept age of 1000 + 14/-11 Ma on zircons extracted from paragneiss from Jetty Peninsula (Fig. 2) and inferred that the dominant regional gneissosity, $S_1/S_0$ (Table I), developed at this time. These data indicate that regional high-grade metamorphism was well advanced by this time but earlier high-grade activity associated with this metamorphic event cannot be precluded.

Synchronous with, or immediately following, peak metamorphism, voluminous felsic magmas of both crustal and upper-mantle affinities (Sheraton *et al.* 1996) were emplaced into the nPCM. Thost & Hensen (1992) and Fitzsimons & Thost (1992) constrain the relative timing of emplacement of charnockites and garnet leucogneiss bodies to postdate $D_1$–$D_2$ but largely predate $D_3$. Kinny *et al.* (1997) subsequently presented SHRIMP U–Pb zircon ages on the Loewe Massif charnockite and garnet leucogneiss at Mount McCarthy, suggesting an emplacement age of 980 ± 21 Ma and 990 ± 30 Ma respectively. Boger *et al.* (in press) reported a U–Pb zircon age from a syn-$D_2$ granitic sill at Radok Lake, indicating emplacement at 990 ± 18 Ma.

Renewed felsic intrusive activity occurred at around 940–900 Ma. An upper-intercept U–Pb zircon age of 940 +24/-17 Ma from a gneissic leucogranite (Manton *et al.* 1992), for which emplacement is constrained to postdate $D_1$–$D_2$ and predate $D_3$ (Hand *et al.* 1994b), places an upper age limit on the development of $F_3$ structures. The age of $D_3$ development in the Radok Lake area was established by dating syn-$S_3$ boudin-neck melt pockets and $F_3$ axial-planar granitic sheets (for which emplacement is clearly synchronous with intense $D_3$ deformation) at 936 ± 11 Ma and 942 ± 17 Ma respectively (Boger *et al.* in press). Although not clearly related to felsic igneous activity, Th–Pb monazite ages from gneisses from Wall Peak (Fig. 2) also yield ages of 930 ± 28 Ma (Nichols & Fahey 1996). Low-angle ramping during $D_4$ resulted in emplacement of still-hot granulites over amphibolites at Radok Lake, initiating partial melting and formation of clinopyroxene-bearing leucosomes for which a U–Pb zircon age of 900 ± 28 Ma is obtained (Boger *et al.* in press). This *c.* 900 Ma age for $D_4$ thrusting probably represents the final stages of early Neoproterozoic tectonism (Boger *et al.* in press).

In contrast to the available U–Pb zircon data from the nPCM, Hensen *et al.* (1997) reported Sm–Nd garnet–whole rock isochron ages from the Porthos Range (Fig. 2) that cluster near 800 Ma. In addition, Nichols & Fahey (1996) reported a Th–Pb age of 800 ± 16 Ma from monazites in shear zones from Wall Peak (Fig. 2). From these data, Hensen *et al.* (1997) concluded that the western nPCM "was deformed and reheated at *c.* 800 Ma", possibly in an Andean-continental arc tectonic setting, but noted that eastern regions of the nPCM were not affected by this event. Hensen *et al.* (1997) postulated that this event reached temperatures of *c.* 750°C, resulting in growth of garnet (in cordierite–sillimanite gneiss), or extensive isotopic resetting of pre-existing garnet, in basement gneisses. The regional structural and metamorphic manifestation of this *c.* 800 Ma event remain to be identified.

Early Palaeozoic isotope ages are widely reported from across the EAS. Tingey (1982) reported biotite and muscovite Rb–Sr ages that cluster at *c.* 500 Ma (largely from the sPCM), and postulated that an anorogenic thermal event affected the PCM region at this time, accompanied by the emplacement of felsic pegmatites. Similarly, Manton *et al.* (1992) reported a range of early Palaeozoic ages from Jetty Peninsula. These include near concordant U–Pb zircon ages from a post-tectonic pegmatite (495–506 Ma), a U–Pb monazite age (528 Ma), internal Rb–Sr mineral isochron ages from felsic syn-tectonic intrusives (*c.* 483–480 Ma) and lower intercepts of zircon discordia from several samples (336–524 Ma). These ages led Manton *et al.* (1992) also to suggest a regional thermal perturbation, associated felsic intrusive activity, and the disturbance of older isotopic systems occurred during the early Palaeozoic.

The recognition of pervasive early Palaeozoic granulite-facies metamorphism and tectonism in nearby Prydz Bay led several workers to suggest the possibility of significant early Palaeozoic metamorphism in the nPCM. For example, in order to explain the complex *P–T* path of Else Platform (Fig. 2), which involved cooling from peak *P–T* conditions and subsequent reheating to low-*P* granulite conditions, Hand *et al.* (1994a), proposed two models. In one, this *P–T* path was the result of fluctuating thermal conditions during the *c.* 1000 Ma event whereas in the second, two unrelated, high-grade events, one at *c.* 1000 Ma and a second at *c.* 500 Ma were superposed. Although Hand *et al.* (1994a) preferred the former model, the latter prompted speculation by Carson *et al.* (1996) and Scrimgeour & Hand (1997) that eastern margins of the nPCM were subject to a high-grade overprint during the early Palaeozoic.

Zhou & Hensen (1995) and Hensen *et al.* (1997) presented Sm–Nd garnet–whole rock ages from Mount McCarthy (Fig. 2). These authors suggested that growth of coronitic garnet in mafic granulite and new garnet in charnockite and leucogneiss occurred at *c.* 630–550 Ma, indicating that the nPCM experienced a significant thermal event at this time. The U–Pb zircon data of Kinny *et al.* (1997) and of Boger *et al.* (in press), however, display a notable lack of *c.* 500 Ma (or *c.* 800 Ma) signatures either as zircon growth (either as rims

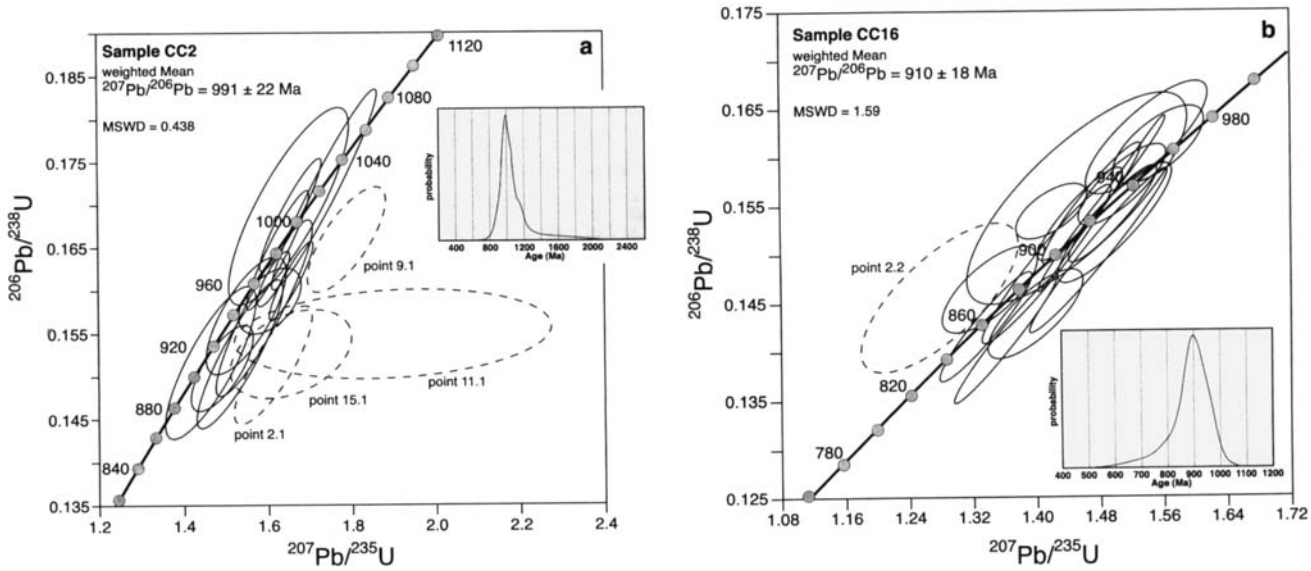


**Fig. 5.** U–Pb Weatherill concordia diagrams showing SHRIMP data for **a**. Sample 2. **b**. Sample 16. Error ellipses are 1 σ. Excluded analyses are indicated by dashed ellipses.

or whole grains), or as lower intercepts, in any of the analysed zircon populations. Both Kinny *et al.* (1997) and Boger *et al.* (in press) reaffirmed the conclusions of Tingey (1982) that the early Palaeozoic event was relatively minor for the most part in the nPCM, disturbing only some mineral isotopic systems and resulting in the development of discrete mylonites and emplacement of felsic pegmatites. High-grade activity of this age appears, at most, limited to the extreme eastern exposures, on Else Platform, where migmatization of post $D_3$ *c.* 500 Ma felsic dykes is reported (Manton *et al.* 1992, Hand *et al.* 1994b).

Most workers conclude that discrete mylonites and pseudotachylytes, common in the nPCM, are structural manifestations of early Palaeozoic activity, although little isotope information explicitly addressing the age of such features is available. Nichols & Fahey (1996) presented isotope evidence that suggests mylonite development at Wall Peak (Fig. 2) at *c.* 800 Ma. Structural, U–Pb and Rb–Sr isotope evidence (Boger unpublished data) indicate two episodes of mylonite formation at Radok Lake, during waning

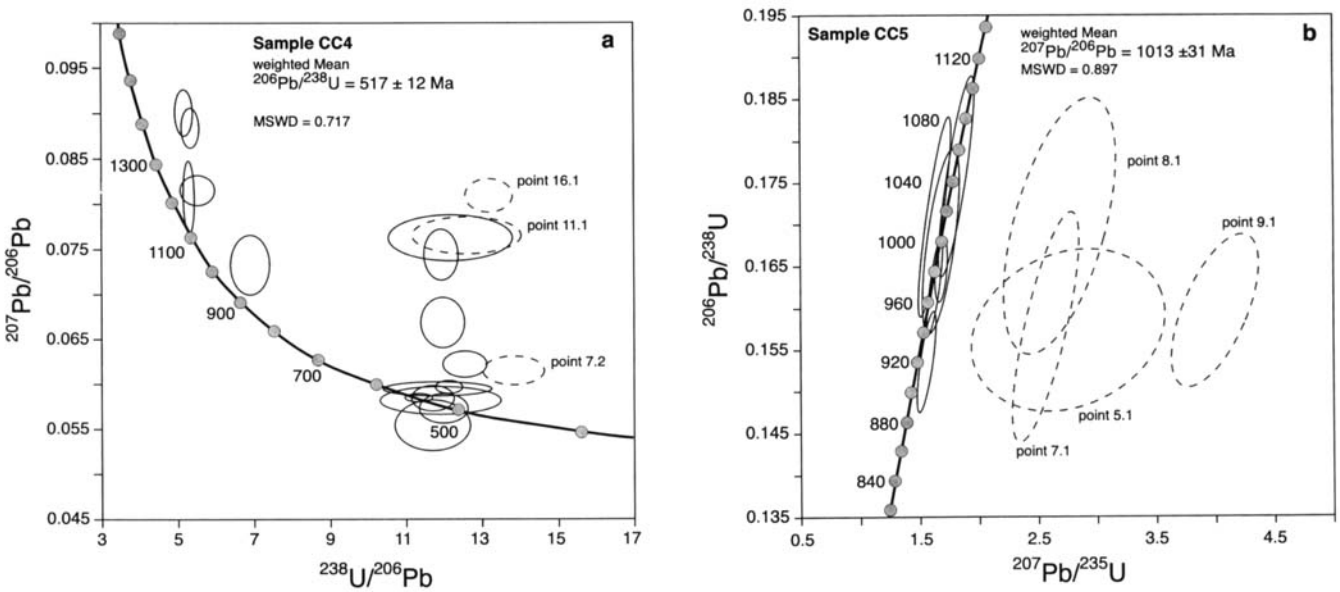


**Fig. 6.** **a**. A U–Pb Tera-Wasserburg diagram showing SHRIMP data for sample 4. **b**. U–Pb Weatherill concordia diagram showing SHRIMP U–Pb data for sample 5. A xenocrystic origin for the analysed zircons is inferred from these data. Error ellipses are 1 σ. Excluded analyses are indicated by dashed ellipses.

https://doi.org/10.1017/S0954102000000523 Published online by Cambridge University Press

**Table II.** Summary of SHRIMP U–Pb zircon results for sample CC2.

| Grain. spot | U (ppm) | Th (ppm) | Th/U | Pb* (ppm) | $^{204}Pb/^{206}Pb$ | $f_{206}$ % | Radiogenic Ratios $^{206}Pb/^{238}U$ | ± | $^{207}Pb/^{235}U$ | ± | $^{207}Pb/^{206}Pb$ | ± | Ages (in Ma) $^{206}Pb/^{238}U$ | ± | $^{207}Pb/^{235}U$ | $^{207}Pb/^{206}Pb$ | ± | Conc. % |
|---|---|---|---|---|---|---|---|---|---|---|---|---|---|---|---|---|---|---|
| 1.1 (rim of type II) | 630 | 394 | 0.63 | 116 | 0.000085 | 0.15 | 0.1698 | 0.0095 | 1.652 | 0.119 | 0.0705 | 0.0028 | 1011 | 53 | 990 | 944 | 82 | 107 |
| 2.1 (rim of type I) | 210 | 530 | 2.53 | 51 | 0.000140 | 0.24 | 0.1513 | 0.0057 | 1.613 | 0.078 | 0.0773 | 0.0020 | 908 | 32 | 975 | 1130 | 53 | 80 |
| 3.1 (type II) | 1478 | 340 | 0.23 | 245 | 0.000031 | 0.05 | 0.1688 | 0.0055 | 1.659 | 0.061 | 0.0713 | 0.0010 | 1006 | 30 | 993 | 965 | 28 | 104 |
| 4.1 (type II) | 1532 | 319 | 0.21 | 245 | 0.000134 | 0.23 | 0.1647 | 0.0057 | 1.627 | 0.063 | 0.0717 | 0.0009 | 983 | 32 | 981 | 976 | 27 | 101 |
| 5.1 (rim of type II) | 425 | 310 | 0.73 | 75 | 0.000414 | 0.71 | 0.1588 | 0.0031 | 1.606 | 0.064 | 0.0734 | 0.0024 | 950 | 17 | 973 | 1024 | 67 | 93 |
| 6.1 (rim of type II) | 590 | 452 | 0.77 | 105 | 0.000355 | 0.60 | 0.1580 | 0.0084 | 1.593 | 0.097 | 0.0731 | 0.0018 | 946 | 47 | 967 | 1017 | 49 | 93 |
| 7.1 (rim of type II) | 1384 | 341 | 0.25 | 221 | 0.000034 | 0.06 | 0.1614 | 0.0027 | 1.616 | 0.033 | 0.0727 | 0.0007 | 964 | 15 | 977 | 1004 | 21 | 96 |
| 8.1 (core of type I) | 352 | 320 | 0.91 | 62 | 0.000132 | 0.23 | 0.1517 | 0.0074 | 1.467 | 0.092 | 0.0701 | 0.0024 | 911 | 41 | 917 | 932 | 71 | 98 |
| 9.1 (type I) | 196 | 537 | 2.74 | 54 | 0.000263 | 0.45 | 0.1660 | 0.0051 | 1.788 | 0.077 | 0.0782 | 0.0021 | 990 | 28 | 1041 | 1151 | 54 | 86 |
| 10.1 (rim of type I) | 347 | 436 | 1.26 | 65 | 0.000132 | 0.23 | 0.1510 | 0.0041 | 1.490 | 0.060 | 0.0716 | 0.0019 | 906 | 23 | 926 | 974 | 56 | 93 |
| 11.1 (rim of type I) | 147 | 335 | 2.28 | 35 | 0.003413 | 5.82 | 0.1549 | 0.0042 | 1.899 | 0.310 | 0.0889 | 0.0140 | 928 | 24 | 1081 | 1402 | 337 | 66 |
| 12.1 (type I) | 537 | 403 | 0.75 | 97 | - | <0.01 | 0.1612 | 0.0037 | 1.658 | 0.044 | 0.0746 | 0.0008 | 964 | 21 | 992 | 1057 | 23 | 91 |
| 13.1 (type II) | 362 | 285 | 0.79 | 64 | 0.000260 | 0.44 | 0.1572 | 0.0057 | 1.550 | 0.080 | 0.0715 | 0.0023 | 941 | 32 | 950 | 972 | 67 | 97 |
| 14.1 (type I) | 508 | 449 | 0.88 | 101 | 0.000118 | 0.20 | 0.1718 | 0.0095 | 1.738 | 0.104 | 0.0734 | 0.0012 | 1022 | 53 | 1023 | 1024 | 34 | 100 |
| 15.1 (type I) | 511 | 447 | 0.88 | 90 | 0.000181 | 0.31 | 0.1527 | 0.0071 | 1.535 | 0.086 | 0.0729 | 0.0019 | 916 | 40 | 944 | 1011 | 53 | 91 |
| 15.2 (type I) | 170 | 407 | 2.39 | 41 | 0.001528 | 2.60 | 0.1526 | 0.0042 | 1.655 | 0.120 | 0.0787 | 0.0050 | 916 | 24 | 992 | 1164 | 132 | 79 |

Uncertainties given at the 1 σ level. $f_{206}$ % denotes the percentage of $^{206}Pb$ that is common Pb. Correction for common Pb made using the measured $^{204}Pb/^{206}Pb$ ratio. For % Conc., 100% denotes a concordant analysis.

Neoproterozoic deformation (*c.* 900 Ma) and again during the early Palaeozoic (550–475 Ma). However, in general, the absolute timing of these discrete features and their role in the tectonic evolution of the nPCM remain somewhat conjectural and elusive.

## Sample descriptions and results

Four samples of structurally-constrained felsic intrusives were selected from Mount Kirkby (Figs 2 & 3) to further constrain the timing of structures associated with high-grade deformation and late discrete mylonite generation in the western Porthos Range. No attempt was made in this study to assess the original protolith ages of the basement orthogneisses. Pegmatites were largely comprised of quartz, plagioclase and K-feldspar. CC16 contained < 5% euhedral garnet. Zircons were separated using standard heavy liquid and magnetic techniques. Grains were hand-picked and selected on the basis of optical clarity and lack of internal fractures. The grains were mounted in epoxy, together with the ANU reference zircon SL13, and were

**Table III.** Summary of SHRIMP U–Pb zircon results for sample CC16.

| Grain. spot | U (ppm) | Th (ppm) | Th/U | Pb* (ppm) | $^{204}Pb/^{206}Pb$ | $f_{206}$ % | Radiogenic Ratios $^{206}Pb/^{238}U$ | ± | $^{207}Pb/^{235}U$ | ± | $^{207}Pb/^{206}Pb$ | ± | Ages (in Ma) $^{206}Pb/^{238}U$ | ± | $^{207}Pb/^{235}U$ | $^{207}Pb/^{206}Pb$ | ± | Conc. % |
|---|---|---|---|---|---|---|---|---|---|---|---|---|---|---|---|---|---|---|
| 1.1 (rim type I) | 1827 | 644 | 0.35 | 287 | 0.000002 | <0.01 | 0.1558 | 0.0069 | 1.480 | 0.068 | 0.0689 | 0.0006 | 933 | 39 | 922 | 896 | 18 | 104 |
| 2.1 (rim type I) | 1790 | 410 | 0.23 | 261 | - | <0.01 | 0.1489 | 0.0067 | 1.414 | 0.068 | 0.0689 | 0.0010 | 895 | 37 | 895 | 896 | 29 | 100 |
| 2.2 (type I) | 1760 | 380 | 0.22 | 249 | 0.000028 | 0.05 | 0.1455 | 0.0063 | 1.279 | 0.082 | 0.0637 | 0.0027 | 876 | 36 | 836 | 733 | 91 | 120 |
| 3.1 (rim type I) | 1543 | 382 | 0.25 | 235 | 0.000039 | 0.07 | 0.1542 | 0.0040 | 1.499 | 0.045 | 0.0705 | 0.0008 | 924 | 23 | 930 | 943 | 24 | 98 |
| 3.2 (core type I) | 1097 | 319 | 0.29 | 156 | 0.000053 | 0.09 | 0.1424 | 0.0045 | 1.336 | 0.048 | 0.0680 | 0.0008 | 858 | 26 | 862 | 869 | 26 | 99 |
| 4.1(rim type I) | 2882 | 357 | 0.12 | 422 | 0.000002 | <0.01 | 0.1544 | 0.0023 | 1.420 | 0.036 | 0.0667 | 0.0013 | 925 | 13 | 897 | 829 | 40 | 112 |
| 4.2 (core type I) | 530 | 495 | 0.93 | 99 | 0.000052 | 0.09 | 0.1611 | 0.0032 | 1.555 | 0.047 | 0.0700 | 0.0015 | 963 | 18 | 952 | 928 | 43 | 104 |
| 5.1 (rim type I) | 2056 | 316 | 0.15 | 297 | 0.000010 | 0.02 | 0.1504 | 0.0039 | 1.428 | 0.046 | 0.0688 | 0.0012 | 903 | 22 | 901 | 894 | 35 | 101 |
| 6.1 (rim type I) | 2468 | 455 | 0.18 | 338 | 0.000019 | 0.03 | 0.1413 | 0.0053 | 1.363 | 0.054 | 0.0699 | 0.0006 | 852 | 30 | 873 | 927 | 18 | 92 |
| 6.2 (core type I) | 1075 | 1277 | 1.19 | 202 | 0.000192 | 0.33 | 0.1531 | 0.0050 | 1.499 | 0.059 | 0.0710 | 0.0014 | 918 | 28 | 930 | 958 | 39 | 96 |
| 7.1 (rim type I) | 3626 | 441 | 0.12 | 503 | 0.000002 | <0.01 | 0.1463 | 0.0036 | 1.343 | 0.049 | 0.0666 | 0.0016 | 880 | 20 | 865 | 825 | 51 | 107 |
| 8.1 (rim type I) | 1356 | 403 | 0.30 | 195 | 0.000037 | 0.06 | 0.1438 | 0.0037 | 1.399 | 0.049 | 0.0705 | 0.0015 | 866 | 21 | 888 | 944 | 43 | 92 |
| 8.2 (core type I) | 1097 | 310 | 0.28 | 168 | 0.000038 | 0.07 | 0.1541 | 0.0039 | 1.458 | 0.043 | 0.0686 | 0.0009 | 924 | 22 | 913 | 887 | 26 | 104 |
| 9.1 (rim type II) | 1635 | 409 | 0.25 | 250 | 0.000028 | 0.05 | 0.1553 | 0.0050 | 1.471 | 0.052 | 0.0687 | 0.0007 | 930 | 28 | 919 | 891 | 23 | 105 |
| 10.1 (rim type I) | 2213 | 428 | 0.19 | 333 | - | <0.01 | 0.1556 | 0.0090 | 1.452 | 0.113 | 0.0677 | 0.0031 | 932 | 50 | 911 | 859 | 98 | 109 |
| 10.2 (core type I) | 1329 | 407 | 0.31 | 215 | 0.000021 | 0.04 | 0.1619 | 0.0048 | 1.541 | 0.061 | 0.0690 | 0.0016 | 968 | 27 | 947 | 899 | 49 | 108 |
| 11.1 (rim type I) | 1585 | 457 | 0.29 | 237 | 0.000028 | 0.05 | 0.1502 | 0.0069 | 1.479 | 0.071 | 0.0714 | 0.0007 | 902 | 39 | 922 | 970 | 21 | 93 |
| 12.1 (type I) | 1833 | 430 | 0.23 | 282 | 0.000022 | 0.04 | 0.1571 | 0.0035 | 1.510 | 0.044 | 0.0697 | 0.0012 | 940 | 20 | 934 | 920 | 34 | 102 |

Uncertainties given at the 1 σ level. $f_{206}$ % denotes the percentage of $^{206}Pb$ that is common Pb. Correction for common Pb made using the measured $^{204}Pb/^{206}Pb$ ratio. For % Conc., 100% denotes a concordant analysis.

https://doi.org/10.1017/S0954102000000523 Published online by Cambridge University Press

**Table IV.** Summary of SHRIMP U–Pb zircon results for sample CC4.

| Grain. spot | U (ppm) | Th (ppm) | Th/U | Pb* (ppm) | $^{204}Pb/^{206}Pb$ | $f_{206}$ % | Radiogenic Ratios $^{206}Pb/^{238}U$ | ± | $^{207}Pb/^{235}U$ | ± | $^{207}Pb/^{206}Pb$ | ± | Ages (in Ma) $^{206}Pb/^{238}U$ | ± | $^{207}Pb/^{235}U$ | $^{207}Pb/^{206}Pb$ | ± | Conc. % |
|---|---|---|---|---|---|---|---|---|---|---|---|---|---|---|---|---|---|---|
| 1.1 (type I) | 6182 | 106 | 0.02 | 483 | 0.000043 | 0.06 | 0.0854 | 0.0035 | | | | | 528 | 21 | | | | |
| 2.1 (type I) | 5839 | 148 | 0.03 | 452 | 0.000104 | 0.02 | 0.0840 | 0.0091 | | | | | 520 | 54 | | | | |
| 3.1 (type II) | 152 | 123 | 0.81 | 32 | 0.000808 | 1.37 | 0.1849 | 0.0061 | 1.9607 | 0.166 | 0.077 | 0.0057 | 1094 | 33 | 1102 | 1119 | 155 | 98 |
| 4.1 (type I) | 4629 | 75 | 0.02 | 347 | 0.000077 | 0.21 | 0.0822 | 0.0020 | | | | | 509 | 12 | | | | |
| 5.1 (type II) | 360 | 285 | 0.79 | 74 | 0.000201 | 0.34 | 0.1809 | 0.0127 | 1.9631 | 0.154 | 0.079 | 0.0021 | 1072 | 70 | 1103 | 1165 | 54 | 92 |
| 6.1 (type I) | 7992 | 275 | 0.03 | 616 | 0.000080 | <0.01 | 0.0835 | 0.0037 | | | | | 517 | 22 | | | | |
| 7.1 (type II) | 216 | 225 | 1.04 | 49 | 0.000318 | 0.54 | 0.1878 | 0.0042 | 1.9780 | 0.119 | 0.076 | 0.0041 | 1109 | 23 | 1108 | 1105 | 110 | 100 |
| 7.2 (type I) | 4397 | 85 | 0.02 | 296 | 0.001217 | 2.83 | 0.0736 | 0.0028 | | | | | 458 | 17 | | | | |
| 8.1 (type I) | 4182 | 92 | 0.02 | 314 | 0.000515 | 2.02 | 0.0821 | 0.0025 | | | | | 508 | 15 | | | | |
| 9.1 (type II) | 228 | 196 | 0.86 | 51 | 0.000370 | 0.62 | 0.1918 | 0.0067 | 2.2458 | 0.119 | 0.085 | 0.0030 | 1131 | 37 | 1196 | 1313 | 71 | 86 |
| 10.1 (type I) | 8504 | 179 | 0.02 | 642 | 0.000527 | 1.10 | 0.0826 | 0.0034 | | | | | 511 | 20 | | | | |
| 11.1 (type I) | 2949 | 40 | 0.01 | 210 | 0.000662 | 2.30 | 0.0775 | 0.0072 | | | | | 481 | 43 | | | | |
| 12.1 (type I) | 3751 | 53 | 0.01 | 289 | 0.000056 | 0.18 | 0.0844 | 0.0085 | | | | | 523 | 51 | | | | |
| 13.1 (type I) | 3940 | 42 | 0.01 | 291 | 0.000978 | 2.25 | 0.0803 | 0.0089 | | | | | 498 | 53 | | | | |
| 14.1 (type II) | 486 | 372 | 0.76 | 79 | 0.000150 | 0.25 | 0.1444 | 0.0091 | 1.4184 | 0.120 | 0.071 | 0.0035 | 869 | 52 | 897 | 964 | 102 | 90 |
| 15.1 (type I) | 1856 | 19 | 0.01 | 134 | 0.000177 | 0.52 | 0.0792 | 0.0032 | | | | | 492 | 19 | | | | |
| 16.1 (type I) | 4390 | 133 | 0.03 | 290 | 0.000213 | 0.43 | 0.0719 | 0.0035 | | | | | 448 | 21 | | | | |
| 17.1 (type I) | 5686 | 96 | 0.02 | 460 | 0.000056 | 0.06 | 0.0884 | 0.0025 | | | | | 546 | 15 | | | | |
| 18.1 (type I) | 1762 | 22 | 0.01 | 140 | 0.000111 | <0.01 | 0.0857 | 0.0061 | | | | | 530 | 36 | | | | |

Uncertainties given at the 1 σ level. $f_{206}$ % denotes the percentage of $^{206}Pb$ that is common Pb. Correction for common Pb made using the measured $^{204}Pb/^{206}Pb$ ratio. For % Conc., 100% denotes a concordant analysis.

sectioned approximately in half and polished. Cathodoluminenscence (CL) imaging was conducted to assess internal zircon structure. Ion microprobe analyses were carried out using SHRIMP(I) at the Research School of Earth Sciences, Australian National University, Canberra, Australia. The SL13 reference zircon standard (which has a radiogenic $^{206}Pb/^{238}U$ ratio of 0.0928) was analysed together with the unknowns. Analytical procedures and data treatment are described in Compston *et al.* (1992). Age calculations have been made using ISOPLOT of Ludwig (1999). The error ellipses shown in Figs 5 & 6 and the errors listed in Tables II–V are at the one sigma level, the mean pooled ages quoted are at the two sigma level following Ludwig (1999).

Sample CC2 is an extensively recrystallized pegmatite, strongly deformed and attenuated by the locally intense upright $S_3$ fabric (Fig. 4c). On close inspection, the pegmatite locally cross-cuts $S_3$ at an acute angle and is therefore inferred to have intruded early syn-$D_3$. Zircons from this sample form two morphological sub-populations. Type I zircons are subhedral to irregularly rounded grains 250–350 μm in diameter with some minor development of terminal facets. They are typically unzoned under transmitted light with a honey to clear colouration and show a varied CL response of complex mosaic patterning. Type II zircons are euhedral with faceted terminations that may or may not contain dark fractured inclusion-rich cores. Under CL, type II cores (which were not analysed) appear as complex mosaics with variable CL response, truncated by euhedral overgrowths with dull to dark

**Table V.** Summary of SHRIMP U–Pb zircon results for sample CC5.

| Grain. spot | U (ppm) | Th (ppm) | Th/U | Pb* (ppm) | $^{204}Pb/^{206}Pb$ | $f_{206}$ % | Radiogenic Ratios $^{206}Pb/^{238}U$ | ± | $^{207}Pb/^{235}U$ | ± | $^{207}Pb/^{206}Pb$ | ± | Ages (in Ma) $^{206}Pb/^{238}U$ | ± | $^{207}Pb/^{235}U$ | $^{207}Pb/^{206}Pb$ | ± | Conc. % |
|---|---|---|---|---|---|---|---|---|---|---|---|---|---|---|---|---|---|---|
| 1.1 | 373 | 438 | 1.18 | 75 | 0.000098 | 0.17 | 0.1639 | 0.0028 | 1.682 | 0.044 | 0.0744 | 0.0013 | 979 | 15 | 1002 | 1053 | 36 | 93 |
| 2.1 | 496 | 528 | 1.07 | 97 | 0.000108 | 0.19 | 0.1626 | 0.0050 | 1.629 | 0.058 | 0.0726 | 0.0011 | 971 | 28 | 981 | 1004 | 30 | 97 |
| 2.2 | 309 | 354 | 1.15 | 64 | 0.000376 | 0.64 | 0.1709 | 0.0098 | 1.619 | 0.112 | 0.0687 | 0.0022 | 1017 | 54 | 978 | 890 | 67 | 114 |
| 3.1 | 427 | 466 | 1.09 | 80 | - | <0.01 | 0.1537 | 0.0051 | 1.552 | 0.069 | 0.0733 | 0.0019 | 922 | 28 | 951 | 1021 | 53 | 90 |
| 4.1 | 414 | 468 | 1.13 | 90 | 0.000045 | 0.08 | 0.1754 | 0.0099 | 1.809 | 0.122 | 0.0748 | 0.0023 | 1042 | 55 | 1049 | 1063 | 63 | 98 |
| 4.2 | 353 | 371 | 1.05 | 70 | 0.000026 | 0.05 | 0.1653 | 0.0044 | 1.658 | 0.052 | 0.0728 | 0.0010 | 986 | 24 | 993 | 1008 | 29 | 98 |
| 5.1 | 34 | 40 | 1.18 | 7 | 0.000195 | 0.34 | 0.1577 | 0.0113 | 2.564 | 0.246 | 0.1180 | 0.0065 | 944 | 63 | 1290 | 1926 | 103 | 49 |
| 6.1 | 271 | 282 | 1.04 | 54 | 0.000391 | 0.67 | 0.1680 | 0.0091 | 1.669 | 0.139 | 0.0721 | 0.0041 | 1001 | 50 | 997 | 988 | 121 | 101 |
| 7.1 | 35 | 40 | 1.12 | 8 | 0.002798 | 4.80 | 0.1572 | 0.0079 | 2.758 | 0.673 | 0.1273 | 0.0296 | 941 | 44 | 1344 | 2060 | 481 | 46 |
| 8.1 | 27 | 26 | 0.97 | 6 | 0.001402 | 2.40 | 0.1698 | 0.0126 | 2.698 | 0.392 | 0.1152 | 0.0134 | 1011 | 70 | 1328 | 1883 | 225 | 54 |
| 9.1 | 38 | 30 | 0.79 | 9 | 0.000728 | 1.25 | 0.1596 | 0.0075 | 3.999 | 0.315 | 0.1817 | 0.0104 | 954 | 42 | 1634 | 2669 | 98 | 36 |

Uncertainties given at the 1 σ level. $f_{206}$ % denotes the percentage of $^{206}Pb$ that is common Pb. Correction for common Pb made using the measured $^{204}Pb/^{206}Pb$ ratio. For % Conc., 100% denotes a concordant analysis

https://doi.org/10.1017/S0954102000000523 Published online by Cambridge University Press

CL response. Zircons from CC2 typically contain *c.* 200 to 1500 ppm U, Th/U ranges from 0.23 to 2.74 (Table II). The isotope data from sample CC2 are presented in Table II. Fifteen zircons grains from this sample were analysed which yield a mean $^{207}Pb/^{206}Pb$ age of 1015 ± 27 Ma (MSWD = 1.72). These results are displayed in Fig. 5a. Grains 2.1, 9.1, 11.1 and 15.2 are highly discordant and are distinct in that they have relatively high Th/U of 2.28–2.74. If these analyses are removed from the population the remaining data give a mean $^{207}Pb/^{206}Pb$ age of 991 ± 22 Ma (MSWD = 0.438), which is taken as the age of crystallization of the pegmatite.

Sample CC16 is taken from a set of south-dipping granitic dykes that are up to several metres wide at Mount Kirkby (Fig. 4d). These felsic dykes clearly crosscut the high-grade structures at a high angle, but are weakly to moderately folded by $D_3$, with a moderate internal $S_3$ foliation defined by flattened quartz and feldspar, parallel to the intense upright $S_3$ foliation preserved in the host gneiss. Late syn-$D_3$ emplacement is inferred.

Zircons from CC16 form two morphological sub-populations. The dominant group (I) is euhedral with faceted terminations and subtle optical zoning, occasionally hosting small rounded fractured cores. Type II zircons are clear, glassy, rounded, multifaceted grains that are unzoned in transmitted light. Analysed zircons from CC16 typically contain *c.* 1000 to 2000 ppm U, Th/U ranges from 0.12 to 1.19 (Table III) with the majority of Th/U around 0.2–0.3, near typical values for magmatic zircon. Twelve zircon grains were analysed, yielding a mean $^{207}Pb/^{206}Pb$ age of 910 ± 18 Ma (Fig. 5b). Removal of the negatively discordant analysis 2.2 does not significantly affect the resultant mean $^{207}Pb/^{206}Pb$ age of 910 ± 18 Ma (MWSD of 1.59) which is taken as the crystallization age of the pegmatite.

Two additional pegmatites were also sampled and analysed (CC4 & 5, Fig. 4e & f). Both pegmatites are planar and are undeformed, either by the dominant gneissosity, $S_1/S_0$, $S_3$ high-strain zones or $F_3$ fold structures. However, the margin of CC4 is weakly reworked by a thin mylonite and CC5 is deformed by a wide ultra-mylonite zone, where it is locally extensively recrystallized and mylonitized. Both these samples therefore place a maximum relative age limit on mylonite development at Mount Kirkby. Zircons from sample CC4 contain high-U euhedral elongate grains (250 x 75 μm), which have a low, homogenous CL response and are uniform under transmitted light (type I). These grains in some cases host small, rounded, highly fractured, cores (100–150 μm in diameter) which are honey-coloured to clear with a bright, mosaic-patterned CL response (type II). These also exist as isolated grains not mantled by elongate zircon growth. The euhedral grains and cores have distinct compositions. The high-U, low response CL zircons from CC4 contain 1762–8504 ppm U with Th/U of 0.01–0.03, whereas cores have 152–486 ppm U and Th/U of 0.76–1.04 (Table IV). Results of all the analysed zircons (18) from CC4 are shown on a Tera-Wasserburg plot in Fig. 6a and tabulated in Table IV. The older Proterozoic ages are derived from type II zircons clearly represent xenocrysts inherited from the enclosing high-grade gneiss, whereas the euhedral elongate zircons with high-U, low Th/U represent a younger, early Palaeozoic, overgrowth. Of the younger group, all the analyses give a mean $^{206}Pb/^{238}U$ age of 505 ± 17 Ma (MSWD = 2.04). The removal of analyses 7.2, 11.1 and 16.1 (with slightly younger $^{206}Pb/^{238}U$ ages of *c.* 450–480 Ma) resulted in a mean $^{206}Pb/^{238}U$ age of 517 ± 12 Ma (MSWD = 0.717) which is taken to represent the crystallization age of the pegmatite.

Zircons from CC5 are well rounded to subhedral grains, 200–300 μm in diameter, honey-coloured to clear in appearance, occasionally with small, rounded, highly fractured, cores. A thin, low U (27–38 ppm) and Th (26–40 ppm) rim with very bright CL response may be present in some cases but produced highly discordant results. The remaining analysed grains have a dull uniform CL response and have U contents ranging from 271–496 ppm with Th/U of 1.04–1.18. Only nine zircons were analysed. Compositional data are presented in Table V and illustrated in Fig. 6b. The highly fractured cores were not analysed. Highly discordant analyses 5.1, 7.1, 8.1 and 9.1 were removed from the population (Fig. 6b), which yielded a mean $^{207}Pb/^{206}Pb$ age of 1013 ± 31 Ma (MSWD = 0.897). It should be stressed that this is a small population of analyses, but sufficient to indicate that the zircons were probably inherited from the adjacent high-grade gneisses. Unfortunately, no pegmatite emplacement age could be inferred from these analyses.

## Discussion

The results obtained for Mount Kirkby are consistent with published U–Pb zircon data from nearby Mount McCarthy and the eastern nPCM. The age of the inherited zircon population from pegmatite CC5 from Mount Kirkby (1013 ± 31 Ma) is consistent with Rb–Sr whole rock ages of *c.* 1000 Ma (Tingey 1982) and the U–Pb zircon age of 1000 +14/-11 Ma (Manton *et al.* 1992) previously reported from the nPCM. These data indicate that regional high-grade metamorphism was well advanced by this time. The emplacement of early syn-$D_3$ pegmatite at 991 ± 22 Ma (CC2), compares with the emplacement ages reported for voluminous pre-$D_3$, charnockite and leucogneiss bodies at Loewe Massif and Mount McCarthy (980 ± 21 Ma, 990 ± 30 Ma respectively, Kinny *et al.* 1997) and syn-$D_2$ granitic sills at Radok Lake (990 ± 18 Ma, Boger *et al.* in press). The relative timing of emplacement of pegmatite CC2 also indicates that local $S_3$ development had commenced by this time. This period of extensive felsic intrusive activity is thought to have been synchronous with, or immediately following, peak granulite-facies metamorphism.

In the western nPCM, the emplacement of the south-dipping pegmatites at Mount Kirkby (CC16) occurred at 910 ± 18 Ma. The south-dipping pegmatites, weakly to moderately deformed by $D_3$, suggest that $D_3$ was still active at 910 ± 18 Ma, although the lack of intense deformation suggests that structural activity

https://doi.org/10.1017/S0954102000000523 Published online by Cambridge University Press

was waning. Although it may be argued that subsequent reactivation of $S_3$ might have occurred significantly after 910 ± 18 Ma, during some later metamorphic event (*c.* 800 Ma or *c.* 500 Ma) which might have been responsible for the weak deformation experienced by the south-dipping pegmatites, there are two lines of argument that contradict this. Firstly, if any such later reactivation were low-grade, then retrogression of the granulite-facies assemblages defining $S_3$ might be expected. This is not observed. Secondly, if any later reactivation of $S_3$ occurred at sufficiently elevated conditions as to form garnet in cordierite–sillimanite bearing assemblages (as proposed by Hensen *et al.* 1997 for the *c.* 800 Ma event), one might expect some disturbance in the zircon isotopic systems and evidence of a *c.* 800 Ma zircon signature, which is not observed or, at least, not recognized. It is reasonable to conclude, on the available U–Pb evidence, that the emplacement of CC16 occurred at 910 ± 18 Ma synchronous with waning $S_3$ deformation.

The available U–Pb data from across the nPCM indicate two broad magmatic/thermal episodes, 1) the emplacement of voluminous felsic magmas during, or near, the metamorphic peak at *c.* 990–980 Ma (e.g. Kinny *et al.* 1997), and 2) a period of less extensive magmatic activity at *c.* 940–900 Ma (Manton *et al.* 1992, Boger *et al.* in press, this study). A similar broadly bimodal distribution of ages is indicated from the Mawson Coast. Young & Black (1991) reported SHRIMP U–Pb zircons ages from the Mawson Charnockite, located near Mawson station (Fig. 2) indicating emplacement at 985 ± 29 Ma and 954 ± 12 Ma. A gneissic xenolith in the Mawson Charnockite recorded zircon growth at 921 ± 19 Ma, this age being interpreted by Young & Black (1991) to reflect zircon growth during deformation and metamorphism rather than of magmatic derivation. Similarly, Dunkley (1998) reported two distinct age populations in SHRIMP U–Pb zircon data from the Cape Bruce region of the Mawson Coast (Fig. 1) with pre-$D_3$ felsic orthogneiss emplacement at *c.* 992 Ma and subsequent growth of zircon in several lithologies at *c.* 910 Ma. Also, Grew *et al.* (1988) reported the emplacement of syn-tectonic pegmatites at 940 ± 80 Ma from the Mawson Coast. These spread of ages, combined with observations on the evolution of high-grade structural features at Radok Lake, led Boger *et al.* (in press) to conclude that the high-grade metamorphic event at "*c.* 1000 Ma" was prolonged and remained continuously active for up to *c.* 100 Ma. The data presented here suggest that *c.* 1000 Ma tectonism, though much reduced in intensity, was still active at 910 ± 18 Ma. However, it remains unclear, at this point, whether the event was continuous or episodic.

### *Early Palaeozoic tectonic activity*

Defining the precise role and intensity of early Palaeozoic activity in the tectonic evolution of the nPCM has proven somewhat elusive. At Mount Kirkby, early Palaeozoic (517 ± 12 Ma) pegmatites are reworked by discrete mylonites (Fig. 4e). Such pegmatites therefore provide a maximum limit on the age of mylonite development at this location. In the Radok Lake region, isotopic evidence suggest two distinct generations of mylonites. South-directed thrusting of nPCM granulites over lower grade units at Radok Lake resulted in the formation of low-angle mylonites at 900 ± 28 Ma (Boger *et al.* in press). Subsequently, on the southern flank of Loewe Massif (Fig. 2), a pegmatite with an U–Pb zircon age of 545 ± 4 Ma is deformed by a later discrete mylonite (Boger unpublished data) providing maximum limits on discrete mylonite development to < 545 ± 4 Ma. However, in the light of the available U–Pb isotopic data, it seems likely that the effects of early Palaeozoic tectonism within the majority of the nPCM is limited to relatively minor thermal and magmatic effects (Tingey 1982), limited mylonite development, and, in places, garnet growth (Hensen *et al.* 1997).

The available structural data suggest early Palaeozoic (< 517 ± 12 Ma) mylonites at Mount Kirkby developed in a local extensional regime (Fig 3). Mylonites of broadly similar age at Radok Lake (*c.* 550–475 Ma, Boger unpublished data) formed in a compressional regime with the axis of compression (Z) sub-parallel to the axis of maximum extension (X) at Mount Kirkby. This deformation in the nPCM was broadly contemporaneous with pervasive compressional granulite-facies deformation (Dirks & Hand 1995, Carson *et al.* 1996) of early Palaeozoic age (*c.* 515–535 Ma, Zhao *et al.* 1992, Hensen & Zhou 1995, Fitzsimons *et al.* 1997) in southern Prydz Bay. Within this framework, we suggest that extensional mylonites recognized at Mount Kirkby (and possibly Wall Peak, Nichols 1995) may be related to isolated block extrusions in a crustal-scale compressional regime that prevailed as a result of the merging of west and east Gondwana during the early Palaeozoic (e.g. Stern 1994).

### *The "c. 800 Ma" event*

Substantial evidence exists for tectonic and/or felsic magmatic activity of this age in adjacent Gondwana fragments, particularly southern and central Africa (e.g. Barton *et al.* 1993, Wilson *et al.* 1993, Pinna *et al.* 1993) and elsewhere in the EAS (e.g. Black *et al.* 1987, Shiraishi *et al.* 1997). Although Th–Pb monazite ages of *c.* 800 Ma from mylonites located at Wall Peak (Nichols & Fahey 1996) suggests mylonite development at this time, the existence of a high-grade event in the western nPCM at *c.* 800 Ma (e.g. Hensen *et al.* 1997) is not supported on the basis of available zircon U–Pb evidence.

## Conclusions

The data presented here are consistent with previous U–Pb zircon studies from the nPCM region. A period of pegmatitic felsic intrusive activity at around 990 Ma occurred synchronously with regional emplacement of voluminous mantle- and locally-derived felsic magma (Kinny *et al.* 1997, Sheraton *et al.* 1996, Boger *et al.* in press) at, or close to, the

https://doi.org/10.1017/S0954102000000523 Published online by Cambridge University Press

metamorphic peak. The development of an upright to steeply inclined high-strain fabric ($S_3$) had commenced by this time at Mount Kirkby. South-dipping pegmatites at Mount Kirkby were emplaced during waning syn-$D_3$ activity at 910 ± 18 Ma, and correlate with syn-$D_3$ magmatic and tectonic activity identified at Radok Lake (Boger *et al.* in press). Currently available U–Pb zircon data (Kinny *et al.* 1997, Boger *et al.* in press, this study), combined with correlation of high-grade structural features across the nPCM, suggest that high-grade structural evolution in the nPCM occurred over the interval *c.* 1000–910 Ma, although these data do not conclusively permit discrimination between continuous or episodic tectonism. Early Palaeozoic activity at Mount Kirkby appears limited to the emplacement of minor felsic pegmatites at 517 ± 12 Ma. This age provides an upper limit for the time of development of extensional discrete mylonites at Mount Kirkby.

## Acknowledgements

Logistic support was provided by the Australian Antarctic Division and funding was from ASAC grant number 2137 awarded to CJLW. The expeditioners of ANARE during the summer of 1995/96 are thanked for hospitality and assistance during the summer, particularly Matt Godbold who watched over us whilst in the field. Careful and thorough reviews by Ian Miller, Simon Harley and Ian Fitzsimons improved the manuscript. DET publishes with the permission of the Australian Antarctic Division.

## References

ARRIENS, P.A. 1975. Precambrian geochronology of Antarctica. *First Australian Geological Convention, Adelaide 1975, Abstracts* 97–98. Geological Society of Australia.

BARTON, C.M., EVANS, J.A., CARNEY, J.N., CROW, M.J. & SIMANGO, S. 1993. Geological and structural framework of the Zambezi Belt, northeastern Zimbabwe. *In* FINDLAY, R.H., UNRUG, R., BANKS, M.R. & VEEVERS, J.J., *eds. Gondwana Eight, assembly, evolution and dispersal.* Rotterdam: Balkema, 55–68.

BELIATSKY, B.V., LAIBA, A.A. & MIKHALSKY, E.V. 1994. U–Pb zircon ages of the metavolcanic rocks of Fisher Massif (Prince Charles Mountains, East Antarctica). *Antarctic Science*, **6**, 355–358.

BLACK, L.P., HARLEY, S.L., SUN, S.S. & MCCULLOCH, M.T. 1987. The Rayner Complex of East Antarctica: complex isotopic systematics within a Proterozoic mobile belt. *Journal of Metamorphic Geology*, **5**, 1–26.

BOGER, S.D., CARSON, C.J., WILSON, C.J.L. & FANNING, C.M. In press. Neoproterozoic deformation in the northern Prince Charles Mountains, east Antarctica: evidence for a single protracted orogenic event. *Precambrian Research.*

CARSON, C.J., FANNING, C.M. & WILSON, C.J.L. 1996. Timing of the Progress Granite, Larsemann Hills: further evidence for early Palaeozoic orogenesis within the east Antarctic Shield and implications for Gondwana assembly. *Australian Journal of Earth Sciences*, **43**, 539–553.

COMPSTON, W., WILLIAMS, I.S., KIRSCHVINK, J.L., ZHANG, Z. & MA, G. 1992. Zircon U–Pb ages for the Early Cambrian time-scale. *Journal of the Geological Society, London*, **149**, 171–184.

CROWE, W. 1994. Geology, metamorphism and petrogenesis of the Fisher terrane, Prince Charles Mountains. East Antarctica. MSc thesis, Australian National University, Canberra. [Unpublished]

DIRKS, P.H.G.M. & HAND, M. 1995. Clarifying temperature–pressure paths via structures in granulites from the Bolingen Islands, Antarctica. *Australian Journal of Earth Sciences*, **42**, 157–172.

DUNKLEY, D.J. 1998. The Rayner Complex in MacRobertson Land, East Antarctica. PhD thesis, University of Sydney, Sydney. [Unpublished]

FITZSIMONS, I.C.W. & THOST, D.E. 1992. Geological relationships in high-grade basement gneiss of the northern Princes Charles Mountains, East Antarctica. *Australian Journal of Earth Sciences*, **39**, 173–193.

FITZSIMONS, I.C.W. & HARLEY, S.L. 1992. Mineral reaction textures in high-grade gneisses: evidence for contrasting pressure–temperature paths in the Proterozoic Complex of East Antarctica. *In* YOSHIDA, Y., KAMINUMA, K. & SHIRAISHI, K., *eds. Recent progress in Antarctic earth science.* Tokyo: Terra Scientific Publishing Company, 103–111.

FITZSIMONS, I.C.W. & HARLEY, S.L. 1994a. The influence of retrograde cation exchange on granulite *P–T* estimates and a convergence technique for the recovery of peak metamorphic conditions. *Journal of Petrology*, **35**, 543–576.

FITZSIMONS, I.C.W. & HARLEY, S.L. 1994b. Garnet coronas in scapolite–wollastonite calc-silicates from East Antarctica: application and limitations of activity-corrected grids. *Journal of Metamorphic Geology*, **12**, 761–777.

FITZSIMONS, I.C.W., KINNY, P.D. & HARLEY, S.L. 1997. Two stages of zircon and monazite growth in anatectic leucogneiss: SHRIMP constraints on the duration and intensity of Pan-African metamorphism in Prydz Bay, East Antarctica. *Terra Nova*, **9**, 47–51.

FITZSIMONS, I.C.W. 2000. A review of tectonic events in the East Antarctic Shield, and their implications for Gondwana and earlier supercontinents. *Journal of African Earth Sciences*, **31**, 3–23.

GREW, E.S., MANTON, W.I. & JAMES, P.R. 1988. U–Pb data on granulite facies rocks from Fold Island, Kemp Land, East Antarctica. *Precambrian Research*, **42**, 63–75

HAND, M., SCRIMGEOUR, I., POWELL, R., STÜWE, K. & WILSON, C.J.L. 1994a. Metapelitic granulites from Jetty Peninsula, East Antarctica: formation during a single event or by polymetamorphism. *Journal of Metamorphic Geology*, **12**, 557–573.

HAND, M., SCRIMGEOUR, I., STÜWE, K., ARNE, D. & WILSON, C.J.L. 1994b. Geological observations in high-grade mid-Proterozoic rocks from Else Platform, northern Prince Charles Mountains region, East Antarctica. *Australian Journal of Earth Sciences*, **41**, 311–329.

HARLEY, S.L. & HENSEN, B.J. 1990. Archaean and Proterozoic high-grade terrains of East Antarctica (40–80°E): a case study of diversity in granulite facies metamorphism. *In* ASHWORTH, J.R. & BROWN, M., *eds. High-grade metamorphism and crustal anatexis.* London: Unwin Hyman, 320–337.

HENSEN, B.J. & ZHOU, B. 1995. A Pan African granulite-facies metamorphic episode in Prydz Bay, Antarctica. Evidence from Sm–Nd garnet dating. *Australian Journal of Earth Sciences*, **42**, 249–258.

HENSEN, B.J., ZHOU, B. & THOST, D.E. 1997. Recognition of multiple high-grade metamorphic events with garnet Sm–Nd chronology in the northern Prince Charles Mountains, Antarctica. *In* RICCI, C.A., *ed. The Antarctic region: geological evolution and processes.* Siena: Terra Antarctica, 97–104.

HOFMANN, J. 1991. Fault tectonics and magmatic ages in the Jetty Oasis area, Mac.Robertson Land: a contribution to the Lambert rift development. *In* THOMPSON, M.R.A., CRAME, J.A. & THOMPSON, J.W., *eds. Geological evolution of Antarctica.* Cambridge: Cambridge University Press, 107–112.

KAMENEV, E., ANDRONIKOV, A.V., MIKHALSKY, E.V., KRASNIKOV, N.N. & STUWE, K. 1993. Soviet geological maps of the Prince Charles Mountains, East Antarctic Shield. *Australian Journal of Earth Sciences*, **40**, 501–517.

KINNY, P.D., BLACK, L.P. & SHERATON, J.W. 1997. Zircon U–Pb ages and geochemistry of igneous and metamorphic rocks in the northern Prince Charles Mountains, Antarctica. *AGSO Journal of Australian Geology and Geophysics*, **16**, 637–654.

LUDWIG, K.R. 1999. *User manual for Isoplot/Ex, version 2.10, a geochronological toolkit for Microsoft Excel*. Berkeley Geochronological Centre Special Publication No. 1a.

MANTON, W.I., GREW, E.S., HOFMANN, J. & SHERATON, J.W. 1992. Granitic rocks of the Jetty Peninsula, Amery Ice Shelf area, East Antarctica. *In* YOSHIDA, Y., KAMINUMA, K. & SHIRAISHI, K., *eds. Recent Progress in Antarctic earth science*. Tokyo: Terra Scientific Publishing Company, 179–190.

NICHOLS, G.T. 1995. The role of mylonites in the uplift of an oblique lower crustal section, East Antarctica. *Journal of Metamorphic Geology*, **13**, 223–238.

NICHOLS, G.T. & FAHEY, A. 1996. Preliminary monazite ages of second generation mylonites, Prince Charles Mountains. *Abstracts, 13th Australian Geological Convention*, Canberra, 316.

ONCKEN, O. 1988. Aspects of the reconstruction of the stress history of a fold and thrust belt (Rhenish Massif, Federal Republic of Germany). *Tectonophysics*, **152**, 19–40.

PINNA, P., JOURDE, G., CALVEZ, J.Y., MROZ, J.P. & MARQUES, J.M. 1993. The Mozambique Belt in northern Mozambique: Neoproterozoic (1100–850 Ma) crustal growth and tectonogenesis, and superimposed Pan-African (800–550 Ma) tectonism. *Precambrian Research*, **62**, 1–59.

SCRIMGEOUR, I. & HAND, M. 1997. A metamorphic perspective on the Pan-African overprint in the Amery area of Mac.Robertson Land, East Antarctica. *Antarctic Science*, **9**, 313–335.

SHERATON, J.W., TINDLE, A.G. & TINGEY, R.J. 1996. Geochemistry, origin, and tectonic setting of granitic rocks of the Prince Charles Mountain. Antarctica. *AGSO Journal of Australian Geology and Geophysics*, **16**, 345–370.

SHIRAISHI, K., ELLIS, D.J., FANNING, C.M., HIROI, Y., KAGAMI, Y. & MOTOYOSHI, Y. 1997. Re-examination of the metamorphic and protolith ages of the Rayner Complex, Antarctica: evidence for the Cambrian (Pan-African) regional metamorphic event. *In* RICCI, C.A., *ed. The Antarctic region: geological evolution and processes*. Siena: Terra Antarctica, 79–88.

STEPHENSEN, N.C.N. & COOK, N.D.J. 1997. Metamorphic evolution of calcsilicate granulites near Battye Glacier, northern Prince Charles Mountains, East Antarctica. *Journal of Metamorphic Geology*, **15**, 361–378.

STERN, R.J. 1994. Arc assembly and continental collision in the Neoproterozoic East African orogen: implications for the consolidation of Gondwana. *Annual Review of Earth and Planetary Science*, **22**, 319–351.

THOST, D.E. & HENSEN, B.J. 1992. Gneisses of the Porthos and Athos ranges, northern Prince Charles Mountains, East Antarctica: constraints on the prograde and retrograde P–T path. *In* YOSHIDA, Y., KAMINUMA, K. & SHIRAISHI, K., *eds. Recent Progress in Antarctic earth science*. Tokyo: Terra Scientific Publishing Company, 93–102.

TINGEY, R.J. 1981. Geological investigations in Antarctica 1968–1969: The Prydz Bay–Amery Ice Shelf–Prince Charles Mountains area. *Bureau of Mineral resources, Geology & Geophysics, Record*, **1981/34**. [Unpublished]

TINGEY, R.J. 1982. The geologic evolution of the Prince Charles Mountains – an Antarctic Archaean cratonic block. *In* CRADDOCK, C., *ed. Antarctic geoscience*. Madison: University of Wisconsin Press, 455–446.

TINGEY, R.J. 1991. The regional geology of Archaean and Proterozoic rocks in Antarctica. *In* TINGEY, R.J., *ed. The geology of Antarctica*. Oxford: Oxford University Press, 1–73.

WILSON, T.J., HANSON, R.E. & WARDLAW, M.S. 1993. Late Proterozoic evolution of the Zambezi belt, Zambia: Implications for regional Pan-African tectonic and shear displacements in Gondwana. *In* FINDLAY, R.H., UNRUG, R., BANKS, M.R. & VEEVERS, J.J., *eds. Gondwana Eight: assembly, evolution and dispersal*. Rotterdam: Balkema, 69–82.

YOUNG, D.N. & BLACK, L.P. 1991. U–Pb zircon dating of Proterozoic igneous charnockites from the Mawson Coast, East Antarctica. *Antarctic Science*, **3**, 205–216.

ZHAO, Y., SONG, B., WANG, Y., REN, L., LI., J. & CHEN, T. 1992. Geochronology of the late granite in the Larsemann Hills, East Antarctica. *In* YOSHIDA, Y., KAMINUMA, K. & SHIRAISHI, K., *eds. Recent Progress in Antarctic earth science*. Tokyo: Terra Scientific Publishing Company, 155–161.

ZHOU, B. & HENSEN, B.J. 1995. Inherited Sm/Nd isotope components preserved in monazite inclusions within garnets in leucogneiss from East Antarctica and implications for closure temperature studies. *Chemical Geology*, **121**, 317–326.